Evaluating the Land-Atmosphere-Cloud Interaction in HRRR using New York State Mesonet

Lanxi Min[1], David R. Fitzjarrald[1], Yuyi Du[1], Brian E. J. Rose[2], Jia Hong[1,3] and Qilong Min[1]

[1]Atmospheric Sciences Research Center, University at Albany, Albany, New York, USA.

[2]Department of Atmospheric and Environmental Sciences, University at Albany, Albany, New York, USA.

[3]State Key Laboratory of Information Engineering in Surveying, Mapping and Remote Sensing, Wuhan University, Wuhan, Hubei, China.

Corresponding author: Qilong Min (qmin@albany.edu)

Key Points:

- The HRRR model near surface thermodynaic biases are seasonally dependent. A systematic warm and dry bias present during the warm season.
- The summer warm and dry biases over farmland are consistently larger than forest.
- Hydrological bias of spring snow melt might eventually lead to the summer warm and dry biases over farmland.

Abstract

The High-Resolution Rapid Refresh (HRRR) model version 3 meteorological fields were examined using data from New York State Mesonet (NYSM) sites from an entire year. In this work, the land surface, atmosphere and cloud coupling systems are evaluated as an integrated system. The physical processes influencing soil hydrological, surface thermodynamic processes from surface fluxes to boundary layer convection are investigated from both temporal (seasonal and diurnal) and spatial perspectives. Results show that the model 2m surface biases are seasonally dependent, with warm and dry bias present during the warm season, and an extreme cold bias during the night in winter. The summer warm bias includes both a land-surface-induced bias and a cloud-induced bias. Inacurate representation of energy partition and soil hydrological process across different land use types and hydrological bias of spring snow melt in the land surface model is the main source of the land-surface induced bias. A feedback loop linking cloud presence, radiative flux changes and temperature contributes to the cloud-induced bias. The positive solar radiation bias increases from clear sky to overcast sky conditions, beyond simply the lack of aerosols in the current version. The most significant bias occurs during overcast and thick cloud conditions associated with frontal passage and thunderstorms.

1 Introduction

The Understanding land-atmosphere coupling is essential for improving weather forecasts at multiple scales (Betts et al., 2013). Soil and vegetation influence the partition of surface energy fluxes, which in turn affecting planetary boundary layer (PBL) development, convective initiation, cloud development, and precipitation (Pleim et al., 2011; Smirnova et al., 2016; Sun et al., 2017; Lee et al., 2018). Subsequent cloud formation and precipitation modulate the exchange of radiation, heat, and moisture in the boundary layer, a feedback that alters surface thermodynamic conditions (Stull, 1988; Freedman et al., 2001; Betts & Silva Dias, 2010). This complex, nonlinear feedback process has been the topic of numerous simulation and observational studies dealing with the land atmosphere interaction (e.g., Eltahir et al., 1998; Schar et al., 1999; Koster et al., 2004; Koster et al., 2006; Taylor et al., 2012; Williams et al., 2016; Peters et al., 2017). Williams et al. (2016) evaluated the single-column version of Community Land Model (CLM4.5) using observations in the U.S. Southern Great Plains. They found the model underpredicted evaporative fraction and overpredicted the impact of soil moisture, leading to biases in the 2-m air temperature and precipitation. Peters et al. (2017) analyzed the impact of surface moisture on the forecasting of a mesoscale convective system (MCS), finding that the initial onset and subsequent MCS displacement was strongly correlated with the model bias in near-surface humidity.

The HRRR (High-Resolution Rapid Refresh) model was developed to serve the US severe weather and aviation forecasting community by providing frequently updated high-resolution short-range weather forecasts (Benjamin et al., 2016). HRRR is highly flexible to develop many valuable forecast applications, including more accurate predictions of thunderstorms and flooding potential (Bytheway et al., 2017; Katona et al., 2016; Griffin et al., 2017), air quality (James et al., 2018), and renewable energy forecasting (Pichugina et al., 2017; James et al., 2017). The performance of HRRR forecasts in terms of land-atmosphere interaction has been evaluated in previous works (Wagner et al., 2019; Lee et al., 2019). Wagner et al. (2019) evaluated HRRR diurnal variation of convective available potential energy (CAPE)

against-derived CAPE obtained from surface-based Atmospheric Emitted Radiance Interferometer (AERI) measurements, finding that HRRR-forecasted CAPE lagged 2 to 4 hours compared to the observations. This is believed to result from the lack of subgrid-scale clouds in version 1 of the HRRR. Lee et al. (2019) also evaluated the HRRR forecasted near-surface meteorological fields and surface energy balance using measurements from two micrometeorological sites. They found that although HRRR-forecasted near-surface temperature and moisture are in good agreement with observations, there are notable positive biases in sensible heat flux, biases that might lead to modeled precipitation underestimates.

The complex landscape of New York State and its immediate surroundings offer a unique opportunity to study the effects of aerosol-cloud-precipitation interactions on weather systems in complex terrain that rely on strong land-atmosphere coupling . In response to increasingly frequent extreme weather events, the University at Albany, SUNY (UAlbany) developed an Early Warning Severe Weather Detection network. This unique network measurement suite, known as the New York State Mesonet (NYSM), fills a critical need of providing data for in-depth model evaluation. It is well-suited for NWP model evaluations of mesoscale processes and comparison with the NYSM observations forms the basis of this study to evaluate HRRR model performance.

2 Data and Methods

2.1 HRRR

The HRRR is a NOAA hourly updated, cloud-resolving, convection-allowing atmospheric model. Since the operational version of the HRRR (currently HRRRv3) was implemented on 12 July 2018, we will perform one-year evaluation between August 1, 2018 and July 31, 2019. In the HRRRv3, Rapid Update Cycle (RUC) land surface model is used to compute surface heat flux and moisture exchanges (Smirnova et al., 2016). The surface temperature is calculated using surface energy balance, which is controlled by shortwave and longwave radiation budget, and energy partition of sensible and latent heat fluxes. HRRR v3 used the Thompson microphysics scheme with 5 hydrometeor types (cloud water, cloud ice, rain, snow and graupel) which improved the upper level cloud biases compared to the previous version (Thompson & Eidhammer, 2014). To better represent sub-grid scale shallow-cumulus clouds, the MYNN Planetary Boundary Layer Scheme is used, with assumed sub-grid cloud probability distribution functions to determine the subgrid scale cloud mixing ratio, cloud fraction, and the buoyancy flux (Olson et al., 2019). The Rapid Radiative Transfer Model for GCMs (RRTM-G) is used to estimate radiative forcing (Iacono et al., 2008). This study focuses on the short-term (1 to 24 hours) forecast from 0 UTC analyses. To allow for sufficient spin-up time, we emphasize the daytime forecasting and analysis.

2.2 New York State Mesonet (NYSM)

In 2017, UAlbany deployed and operated a dense environmental monitoring network, New York State Mesonet (NYSM, http://nysmesonet.org/). The NYSM has 180 sites with state-of-the-art instrumentations, including 126 standard surface meteorology stations, 17 flux towers and 17 atmosphere profilers, which are the most sophisticated, high density (average distance between stations ~ 26 km) statewide observing network. The 126 standard surface stations measure not only standard meteorological variables (temperature, humidity, wind speed and direction, pressure, and precipitation) but also soil temperature and moisture at three levels, snow

depth, and total surface short-wave (SW) irradiance at 5-minute intervals (Brotzge et al., 2020). The sub-network of 17 enhanced surface energy budget stations directly measure both incoming and outgoing shortwave and longwave radiation, ground heat flux, and turbulent fluxes of momentum, sensible and latent heat, and carbon dioxide with 30 minutes intervals (Covert, 2019). Topography and land use characteristics are considered when selected the flux station locations. To be comparable to HRRR, only data sampled at an hourly interval are used in this paper. As NWP models transit to a high-resolution convection-allowing framework, infrequent atmospheric sounding profiles (currently only 2 soundings per day at three sites within NYS) are inadequate. Recognizing this critical measurement gap, the NYSM operates 17 enhanced atmospheric profiler systems that are sited along population, transportation and utility corridors, strategically positioned to capture upwind features approaching the station (Freedman et al., 2016). Each profiler site is equipped with a wind Doppler LiDAR (WDL), a profiling (multi-frequency) microwave radiometer (MWRP) and the environmental Sky Imager-Radiometer (eSIR). The profiler network continuously samples the vertical profiles of temperature, humidity with MWRP from surface to 10 km (Yang & Min, 2018). MWRP significantly increased temporal resolution of temperature and humidity vertical measurements. Compensated with higher vertical resolution from sounding, MWRP measurements will provide better understanding of boundary layer conditions. eSIR is a dual-measurement system comprised of continuous (daytime) observations of aerosol and cloud optical depths, narrowband spectral direct and diffuse radiation, and whole sky images (cloud distribution and motion for solar energy forecasting). The WDL provides not only 3D wind fields (up to 7 km) but also planetary boundary layer (PBL) height and vertical profile of aerosol optical properties (synergistic with eSIR inferred aerosol optical depth). The multi-frequency MWRP independent information on temperature and moisture, and cloud liquid water--crucial data for determining upper atmospheric conditions (Yang & Min, 2018) and cloud optical properties (Min & Harrison, 1996). This advanced instrument suite provides an unprecedented data stream of aerosols, clouds, radiation, precipitation, multi-level soil moisture/temperature, snow depth/snow water content, surface fluxes, and meteorological profile data at high spatial and temporal resolution, providing the ability to track abrupt changes in thermodynamic profiles throughout the state.

To quantify the cloud conditions at the standard sites where eSIR is not available, the observed global horizontal irradiance (GHI) or total solar radiation was used to calculate the clear-sky index (CSI). The clear-sky index is the ratio of observed GHI to the baseline GHI under clear-sky conditions in that month. A simple clear sky model was used to calculate clear-sky solar radiation (Robledo & Soler, 2000):

$$GHI = A \times (\cos z)^{B} \times \exp\left(C \times \left(90^{0} - z\right)\right) \qquad (1)$$

Where GHI is the Global Horizontal Irradiance; z is solar zenith angle; and A, B, C are the fitting parameters at specific site, derived from GHI measurements of selected clear-sky days in one month. Consequently, the CSI describes the atmospheric clear-sky or cloudy-sky conditions, defined as

$$CSI = \frac{GHI}{GH\,I_{clear-sky}} \qquad (2)$$

Specifically, we classified the weather conditions as:

- Clear-sky conditions with CSI > 0.8.
- Transition conditions with CSI between (0.6, 0.8), in which either optically thin clouds or broken clouds are present in the sky.
- Overcast conditions with CSI <= 0.6.

3 Results

3.1 Temporal and spatial analysis of the HRRR 2-m forecast

The 2-m temperature and relative humidity are key meteorological parameters for diagnosing and evaluating model performance. They are strongly influenced by the coupling processes between land and atmosphere. During the warm season there are consistent warm and dry biases during both daytime and nighttime (Figure 1). The daytime maximum temperature bias, however, is anti-correlated with the bias of the nocturnal minimum temperature ($r \approx -0.49$). This suggests that low-level cloud dynamics might play a direct and important role in the diurnal cycle of the warm season surface temperature bias. During the daytime, low-level clouds tend to block the shortwave radiation and cool the surface. However, at night, the same low-level clouds reduce the outgoing longwave radiation and keep the surface warm. An inaccurate representation of low-level clouds during both daytime and nighttime is a possible reason for the negative correlation. In contrast, both biases of maximum and minimum temperatures during the cold season show no significant systematic biases, with extreme negative biases on the coldest days. The daytime maximum temperature bias and nocturnal minimum temperature bias are positive correlated ($r \approx 0.36$), indicating different physical processes other than low cloud bias controlled the cold season surface biases. In winter, the snow freezing and melting processes largely modulate the surface temperature and humidity. The freezing and thawing processes in the snow cover and soil are possibly responsible for the cold extreme biases (Viterbo et al., 1999; Garc´ıa-D´ıez et al., 2013)

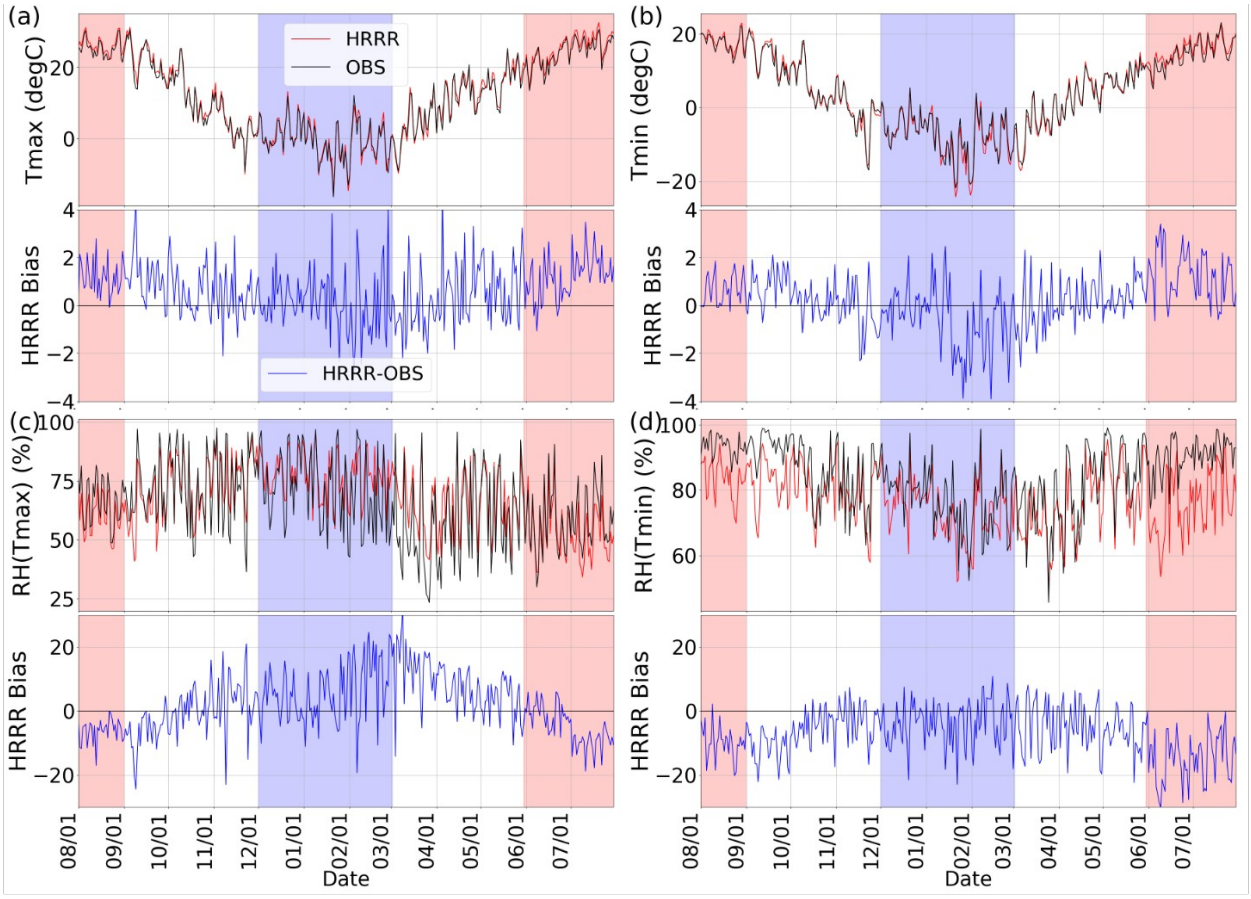

Figure 1. Average time series of data from 126 NYMN sites: (a) daily maximum temperature and (b) is daily minimum temperature; (c) corresponding relative humidity to daily maximum temperature. and (d) corresponding relative humidity to daily minimum temperature.

The HRRR vegetation module incorporates monthly updated MODIS (Moderate Resolution Imaging Spectroradiometer) satellite retrieved vegetation. In New York, the transition seasons (spring, fall) rapidly progress northward in spring or retreat to the south in fall (Fitzjarrald et al., 2001). Significant changes in vegetation "greenness", soil temperature, and soil moisture in a few weeks during leaf emergence coincide with corresponding changes in the surface energy partition. Figure 1 also shows these distinct seasonal transitions in the 2-m temperature and RH bias characteristics that occurred around mid-May (during spring onset and leaf emergence) as well as mid-October (during leaf senescence in New York State), indicating that the HRRR model physics associated with the spring and fall season transition may lack precision. Detailed statistics of daily maximum/minimum temperature and relative humidity for each month are listed in Table 1. These strong seasonality of biases in temperature and RH suggests that there are potential issues with the land-atmosphere coupling in the HRRR.

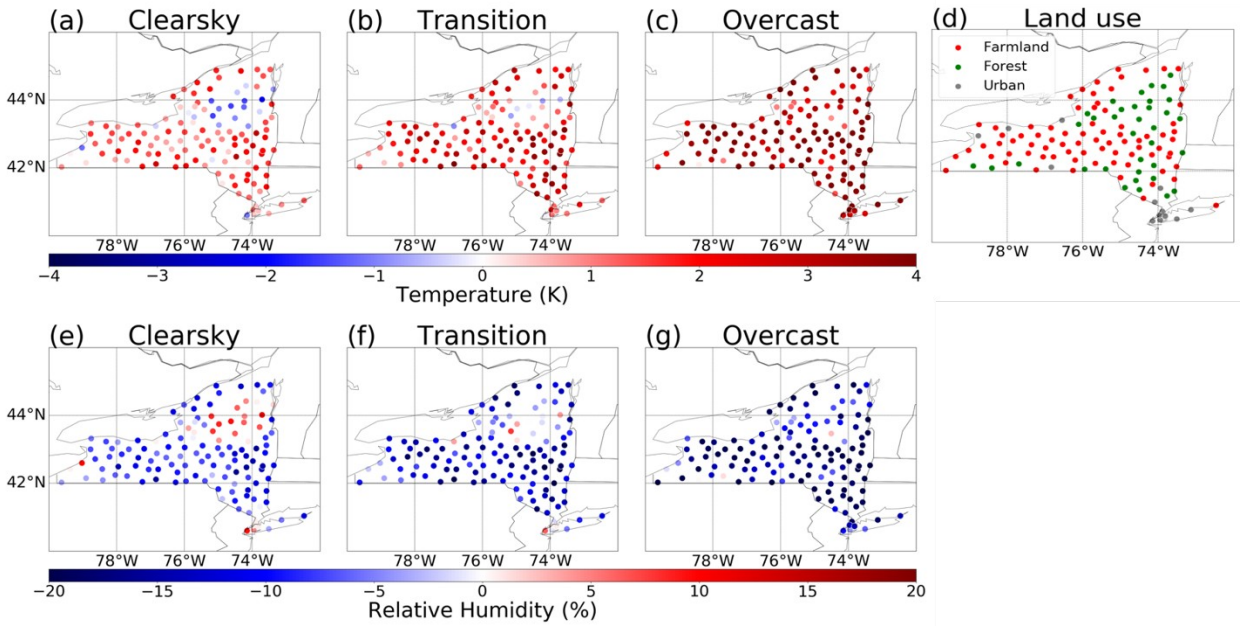

Figure 2. Spatial distribution of the 2-m temperature and RH biases classified by clear sky index in July 2019 over NYSM 126 standard sites: (a) and (e) clear-sky conditions with CSI > 0.8; (b) and (f) transition conditions with CSI between (0.6, 0.8); and (c) and (g) overcast conditions with clear sky index <= 0.6. (hour 0900-1700).

Table 1. Mean Bias Error (MBE), Root Mean Square Error (RMSE) of daily maximum/minimum temperature, relative humidity between 126 standard NYSM sites and the HRRR over period 1 Aug. 2018 to 31 Jul. 2019. Statistics are based on all hourly observations and averaged over monthly and separated by different land use types (farmland and forest)

		Jan	Feb	Mar	Apr	May	Jun	Jul	Aug	Sep	Oct	Nov	Dec
Farmland	Tmax (MBE)	0.17	-0.13	-0.23	0.82	0.92	0.94	1.94	1.33	1.24	0.57	0.32	0.24
	Tmax (RMSE)	1.25	1.70	1.21	1.40	1.14	0.87	0.72	0.74	1.03	0.97	1.02	0.79
	Hmax (MBE)	2.96	10.56	13.91	4.10	1.70	-2.15	-11.23	-7.99	-7.72	0.68	3.17	3.12
	Hmax (RMSE)	7.62	10.24	7.95	9.16	5.45	4.68	3.40	3.75	5.88	5.54	8.41	6.03
Forest	Tmax (MBE)	0.25	-0.07	-0.69	0.05	0.23	0.10	1.07	0.86	1.02	0.67	0.67	0.28
	Tmax (RMSE)	1.26	1.67	1.27	1.60	1.54	1.12	0.93	0.90	0.98	1.10	1.10	0.70
	Hmax (MBE)	3.06	11.45	17.82	12.32	7.61	3.45	-5.69	-3.69	-5.11	-0.12	0.70	1.42
	Hmax (RMSE)	6.65	11.41	10.63	9.08	7.86	6.09	5.54	4.29	6.00	7.82	11.18	7.86

The dense NYSM network enables us to study the HRRR performance, as a function of heterogeneous land covers, and soil conditions under a variety of weather conditions. In the warmest month, (July, 2019), Spatial pattern of 2-m temperature and humidity biases are correlated closely to the land surface types under all weather conditions (Figures 2a-2d). The forest sites, particularly at Adirondack northern plateau forest regions, have lower or even opposite 2-m temperature biases compared to the nearby sites under all weather conditions. Table 1 also shows that in warm season (June, July, August), the mean 2-m temperature biases

are much larger over farmland. The dependence of land use type further illustrates a potential issue in the Rapid Update Cycle (RUC) Land Surface Model (LSM) used by the HRRR. For the warm bias introduced by cloud forcing, it is found that the most significant bias comes form overcast clouds, which indicating that the severe thunderstorm or the synoptic scale cloud are the main source to the warm season surface temperature bias. It is hypothesized that land surface energy partition and cloud forcing are two main factors controlling the warm season surface temperature bias.

3.2 Soil hydrological process in land surface model

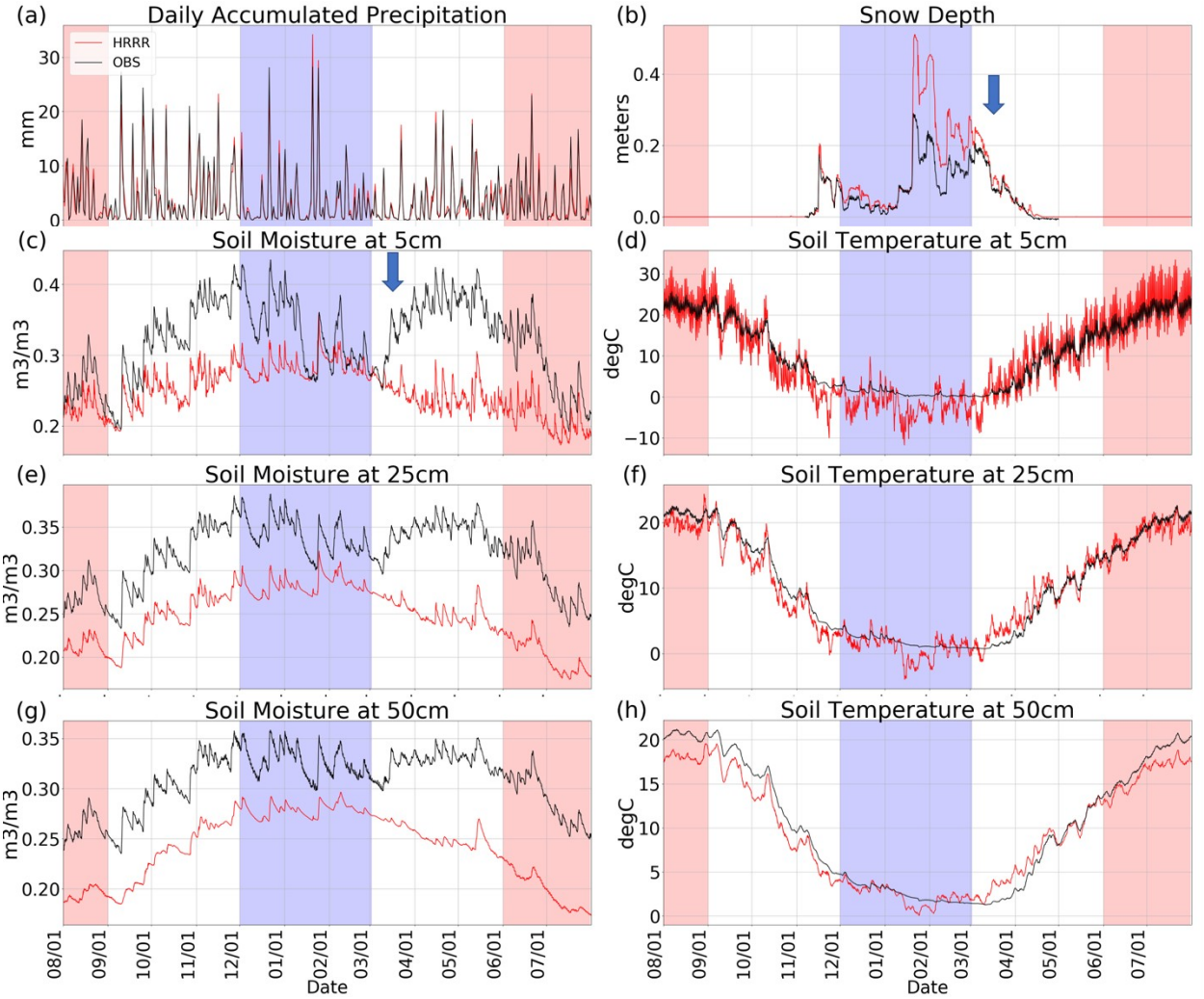

Figure 3. Time series of 126 standard sites averaged (a) daily accumulated precipitation, (b) snow depth, (c, e, g) soil moisture at 0.05 m, 0.25 m and 0.5 m; and (d, f, h) soil temperature at 0.05 m, 0.25 m, 0.5 m.

Soil moisture is an important variable among the processes that describe the land surface–atmosphere coupling. Its value reflects how rainfall is partitioned into runoff, surface storage, and infiltration components. One consequence is that soil moisture modulates the energy budget by determining the soil heat capacity, the degree of evapotransipiration, and the albedo

(Seneviratne et al., 2010; Smirnova et al., 1997; Gascoin et al., 2008). Through balancing of land surface water and energy, soil moisture directly affects 2-m temperature and humidity by controlling the total energy used by latent heat flux, and further modulating surface energy partition. (Kala et al., 2016; Seneviratne et al., 2013; Mueller & Seneviratne, 2014). Soil moisture at all three levels of 0.05 m, 0.25 m, 0.5 m are closely associated with the precipitation. The spikes of precipitation-induced soil moisture increase matches alright between model and observation (Figures 3a, 3c, 3e and 3g).

At each mesonet station, a Stevens Hydra Probe Soil Sensor measures soil moisture based on dielectric permittivity measurements. Proprietary algorithms were used to convect the signal response of the standing radio wave into the dielectric permittivity and thus the soil moisture. The soil moisture measurements are in units of water fraction by volume (m3/m3), which is consistent with model. The forecasted soil moisture values at 0.25 m and 0.5 m have systematic biases around 0.05 m3/m3 respectively. The forecasted soil moisture at 0.05 m showed few apparent biases when compared to NYSM measurements at the beginning of the evaluation period (August, 2018), but a dry bias emerged as the fall transition proceeded (Figure 3c). During the warm days of late winter to early spring, snowmelt, which is the major reason for snow depth reduction, adds water into the soil. NYSM observation shows around 20cm snow melted during early spring and in the meantime, observed soil moisture increased sharply (blue arrow in Figure 3). However, the forecasted soil moisture at 0.05 m did not respond to the snow water as indicated by the NYSM observations. This suggests that the snow melting process is poorly represented by the HRRR, either due to RUC thawing process or due to the snow water runoff.

Changes in soil moisture affects surface temperature and vice versa. HRRR-forecasted soil temperatures at three levels (Figures 3d, 3f and 3h) basically agree with NYSM observations. However, HRRR predicted a much larger diurnal cycle of soil temperature at the 0.05 m and 0.25 m levels than observation (Figures 3d and 3f). One possible reason is that the overall dry biases of soil moisture decreased the soil heat capacity, and led to increased amplitude of soil temperature variation. Also, the observed average soil temperature was above freezing during the cold winter months, while HRRR forecasted soil temperature exhibited much lower temperatures, below freezing (Figure 3d). These examples illustrate potential issues in the RUC as used by the HRRR, including difficulties simulating the soil freeze-thaw processes (Viterbo et al., 1999; Ek et al., 2003). In real world, the water in the soil will not completely freeze, rather remain a mixture of ice and water at the temperature of 0 degree Celsius. However, the model unrealistically freeze the soil during the cold winter. This bias in soil temperature partly explains the extreme cold bias we see earlier in 2m air temperature.

The soil moisture budget examines one avenue of how changes in the land surface may alter the water and energy balances. Precipitation and snowmelt inputs increase soil moisture through infiltration are countered by runoff and evapotranspiration outputs, as evapotranspiration releases water from plant leaves and soil (Figure 4). The comparison between HRRR change rates and NYSM observation in four seasons exhibit unique seasonal characteristics:

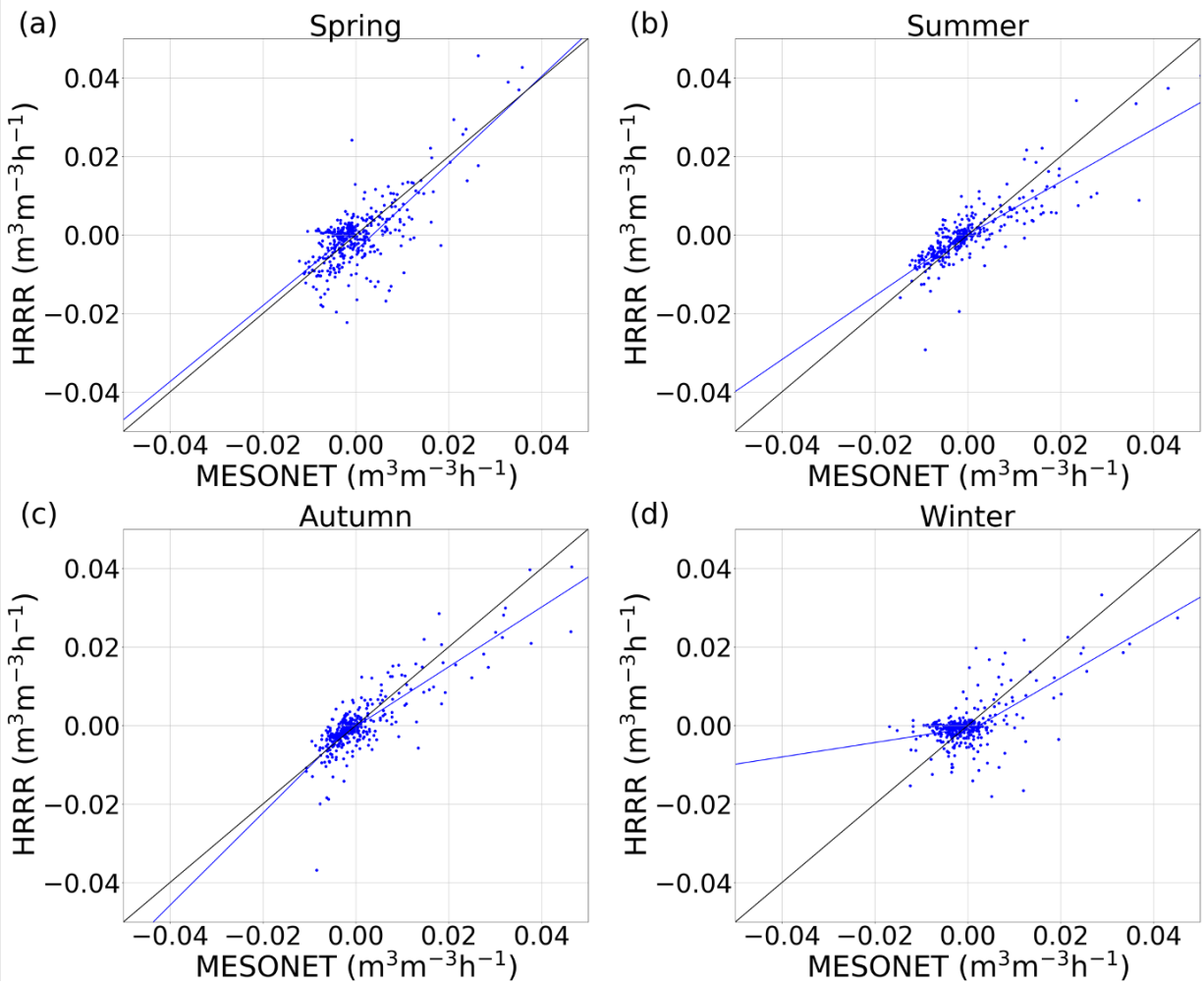

Figure 4. Mesonet observed and HRRR simulated regression fits for soil moisture differential at 0.05 m during different seasons. the growth rate and loss rate are linear fitted separately.

Table 2. Comparison of modeled with observational soil moisture rates of change under different precipitation conditions.

	loss rate			growth rate		
	r	slope	intercept	*r*	slope	intercept
Spring	0.50	0.97	0.0006	0.78	1.11	-0.0040
Summer	0.66	0.81	0.0006	0.78	0.67	0.0001
Autumn	0.59	1.18	0.0012	0.84	0.76	-0.0002
Winter	0.19	0.18	-0.0006	0.66	0.68	-0.0016

• Spring: Snowmelt is important to soil hydrological process for soil moisture growth rate during early spring season. The extreme high intercept -0.0040 $m^3m^{-3}h^{-1}$ shown in Table 2 could be attributed to the misrepresentation of snow melting process. In the mean time, the loss rates of soil moisture during this period are not well captured by HRRR forecasts. The loss rate correlation coefficient r is only 0.50. The result indicates that large uncertainty still lies in the soil hydrological process during spring associated with snow metling and the partition of water into runoff, soil moisture and evapotranspiration.

• Summer: The precipitation has been underestimated in summer with the integrated bias as -20.56 mm in whole summer, which lead to the underestimation of the growth rate of soil moisture forecasted by HRRR in summer (Benjamin et al., 2016). The loss rate of soil moisture forecasted by HRRR tended to be lower than NYSM observation, suggesting a weak evapotranspiration process in HRRR RUC (Figure 4b). A combined result of the underestimation of both growth and loss rates is that the overall soil moisture dry bias decreases from its maximum at the beginning of summer to much less in late summer (Figure 3c). The severely underestimation of evapotranspiration processes changes surface energy patition and lead to the consistent warm bias observed. Land surface biases further affect the convective behavior of boundary layer clouds during summer, creating positive feedbacks in land atmosphere cloud coupling process.

• Autumn: The HRRR underpredicted the growth rate of soil moisture, however, overestimated the loss rate during the transition season. The overestimation of loss rate in fall indicates that the evapotranpiration process during autumn has been overestimated. As leaf senescence occurred in New York during this period, the transpiration went way, the vegetation ceased to withdraw water from the soil. The soil moisture continued to build up and reached its annual maximun in early winter. In Figure 3c, the model shows a gradual dry bias in forecasted soil moisture, with almost the same level of soil moisture at the beginning (September 1st) and 0.1 m3/m3 bias at the end of the fall (November 30th). It is likely that the vegetation phenology changes during the fall and their impact on soil moisture dynamics are not well represented in HRRR RUC.

• Winter: The soil hydrological process is most poorly simulated in winter. The HRRR growth rate of soil moisture is underpredicted, and the loss rate is largely underpredicted. During the winter, precipitation can be either in liquid phase (i.e., rain) which immediately interacts with soil or in solid phase (i.e., snow) accumulated for later release. The soil freezing and thawing processes adds more complexity to the soil moisture dynamics. The observed HRRR biases suggest the needs to further investigate the snow precipitation process, snow-pack dynamic and the soil freeze cycle in the HRRR.

3.3 Surface energy partition

The land use types have a major control on the surface energy partition. The way that the model represents the partition of sensible and latent heat flux with different land use types is crucial to the forecast of land surface meteorological condition and cloud formation through land atmosphere feedbacks. To gain deeper insight into model performance, HRRR forecasted energy partition at three major land use type sites of forest, farmland forest mosaic, and urban are evaluated using the flux measurements from NYSM flux sites. It should be noted that, for three

selected flux sites, however, the immediatedly surrounding area is flat with grassland or low vegetation to meet WMO standards. To get the best representation of heat fluxes from different land use types, only the data from mid-afternoon (1800 UTC) are used. During this period, the impact of surrounding land cover on the flux measurements is most significant due to that the mixing of boundary layer is strongest at this time of the day.

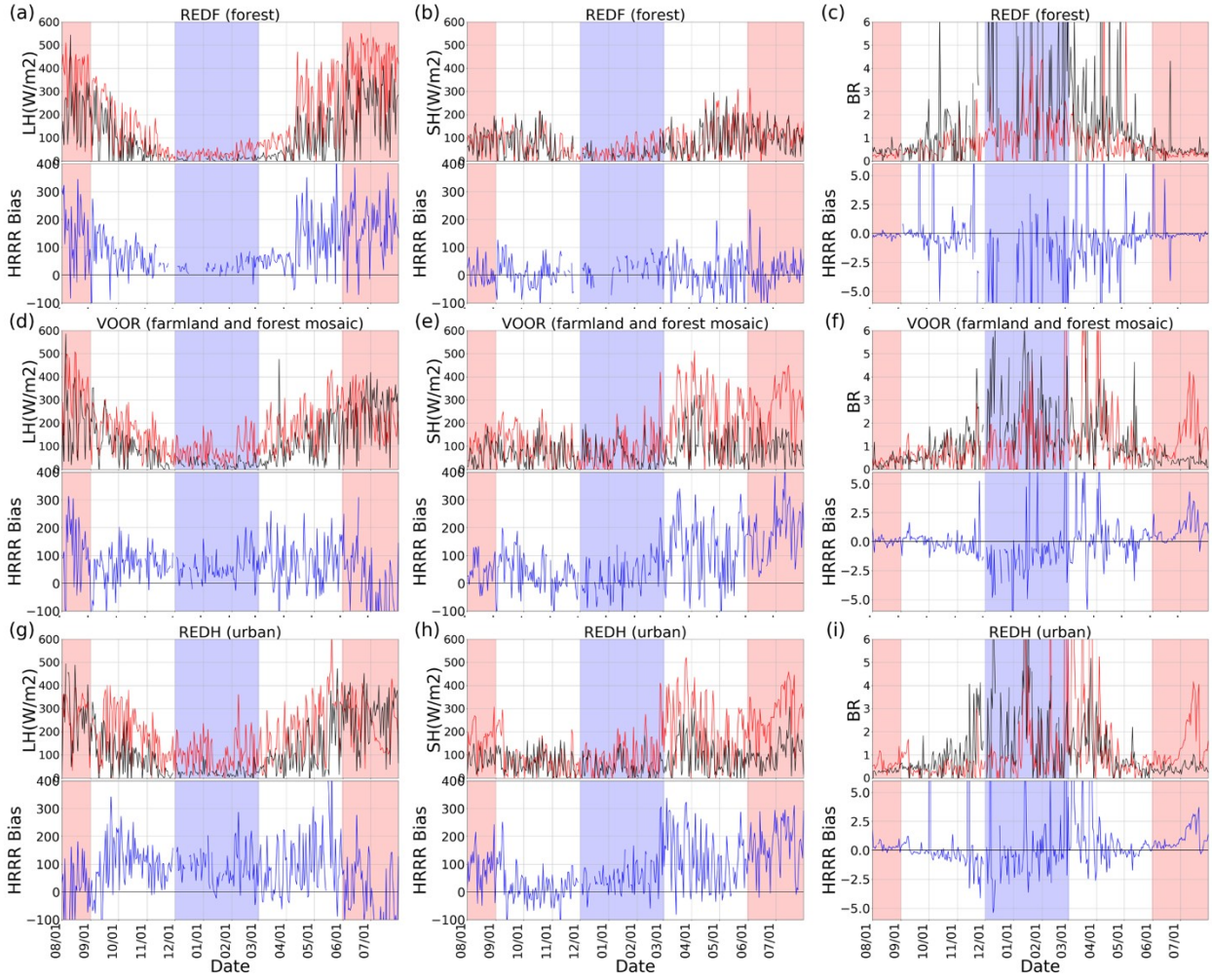

Figure 5. Time series of (a, b, c) daytime latent heat flux, sensible heat flux, Bowen ratio measured from farmland flux sites; and (d, e, f) from forest flux sites.

At forest sites during the warm season, the latent heat flux is overestimated, and the sensible heat flux is close to the measurements. However, considering that the observed fluxes have an estimated 100W/m2 to 200W/m2 energy closure imbalances (Steeneveld et al., 2011), it is possible that the sensible heat flux has been underestimated at the forest sites. HRRR underpredicted the Bowen ratio compared to NYSM observation for most of the growing season, from spring onset to leaf senescence (Figures 5a-5c). The bias in energy partition over forest sites partly explains the slight cold and wet bias over Adirondack region under clear sky shown in Figure 2a. Over the forest, the evapotranspiration process is dominating the latent heat flux during the growing season. The deep rooting system enables the forest to be less affected by the surface soil moisture drought.

On the contrary, the HRRR predictions of Bowen ratio over farmland sites are generally larger than the observation during the warm season. Compared to forest, farmland has a much shallower root depth, which is more vulnerable to the water deficit at surface soil layers. As discussed in section 3.2, soil moisture has been underestimated during the warm season. The false drought in soil further lead to the underestimation of latent heat flux, while sensible heat flux is overestimated around 300 W/m2. This relatively larger biases of Bowen ratio over farmland sites than those over forest sites consist with the larger warm bias of 2-m temperature over farmland sites than those over forest sites (Figure 2). These biases will also contribute to changing of the convection behavior of cloud, and further enlarge the surface thermodynamic bias through surface cloud feedbacks.

During the snowmelt period, HRRR predicted more LH (Figure 5a) without significant increase in soil moisture at 0.05 m level (Figure 3c). In fact, Figure 3c shows that 0.05 m soil moisture in HRRR decreases steadily during this period, while the observation increases rapidly. The result suggests that most melt water was evaporated into the atmosphere and did not infiltrate into the soil.

Over the urban site, the HRRR forecast of energy partition is similar to that of the farmland and forest mosaic sites. The latent heat flux has been underestimated, and sensible heat flux has been overestimated.

As shown in Figure 2 in section 3.1, the 2-m air temperature and humidity bias can be attributed to two sources, the land surface budget and cloud. In this section, the modelled surface heat fluxes over different land use types has been evaluated with observation. During the warm season, the underestimation/overestimation of bowen ratio over forest/farmland sites lead to the cold/warm and wet/dry biases under the clear sky. The dry bias in soil moisture, and underestimation of evapotranspiration during warm season partly explained the bias in surface energy budget. The early spring snow melting problem could be one of the reasons that lead to the warm and dry biaes in the warm season. Under the effect of insufficient water infiltrating into the soil during the spring, the deficit of soil water at the beginning of summer, suppressed the evapotranspiration especially over shallower rooted vegetation and further induce warmer drier surface air.

3.4 Cloud effects on land-atmosphere coupling biases

Underestimation of low-level cloud coverage and optical thickness has been identified as an important potential explanation for the systematic daytime incoming solar radiation bias, in turn yielding a surface warm and dry bias during the warm season (Benjamin et al. 2016). Here the biases of downward shortwave radiation and maximum 2-m air temperature are investigated by classifying biases using clear sky index.

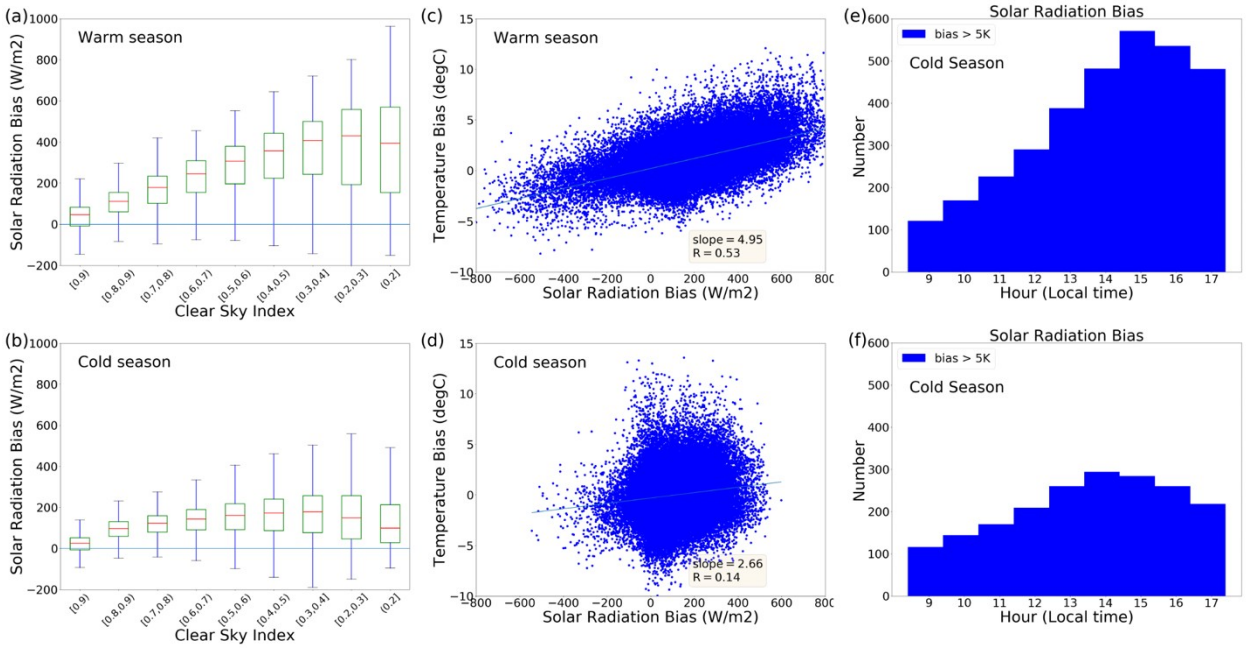

Figure 6. (a,b) Box-and-whisker plots showing the shortwave radiation bias binned by clear sky index (warm/cold season). The vertical bar represents standard error. (c,d) correlations between downward shortwave radiation bias and daily maximum temperature bias; (e, f) Number of measurements in certain hours when the temperature biases exceed 5 K. The warm season is June, July, August (JJA), and the cold season is December, January and February (DJF). Only daytime (from 9:00 to 16:00 local time) data are included in the statistics.

Figure 6a shows that during the warm season, the shortwave radiation bias increases as observed clouds thicken (The clear-sky index in Figure 6 is based on station observation). The dependence of shortwave biases on cloud is more significant in warm season than during the cold season (Figures 6a and 6b). In the warm season, a negative radiation bias around 100 W/m2 when the clear sky index exceeds 0.9. The absence of aerosol direct effect in HRRR could be the reason for this negative bias under clear sky. For clear sky index < 0.2, when the sky is covered by optically thick clouds, the mean radiation bias can be as high as 400 W/m2. In contrast to previous studies that emphasized the importance of unresolved fair-weather sub-grid clouds on the surface temperature bias, our analysis indicates that optically thicker clouds result in the largest radiation bias. During the warm season, the clouds over NEUS can be separated into four categories: Fair weather cumulus, cumulus congestus (towering cumulus), individual cumulonimbus, and stratocumulus associated with thunderstorm and frontal passage. The large bias with low cloud index is associated with type 3, 4 clouds. The displacement and weaker strength in deep convection might explain most of the biases in thick clouds.

During the warm season, daytime temperature bias correlate well with shortwave radiation bias (Figure 6c) . Further analysis separates the radiation and temperature biases using the clear sky index. In both warm and cold seasons, it is clearly shown (Table 3) that the slope of the linear regression between solar radiation and temperature biases decreases as the clear sky index increases, as does the correlation coefficient r. The result further supports the argument that the relationship between radiation bias and temperature bias is more significant with thicker clouds. Compared to the warm season, the cold season daytime temperature bias is much less

dependent on cloud bias. When the clear sky index exceeds 0.4, the slope becomes negative, and the correlation coefficient essentially vanishes. One possible reason is that the surface snow in cold season dominates boundary layer processes instead of shortwave cloud forcing (Betts & Beljaars, 2017). Also, due to the much thinner convective boundary layer, the surface thermodynamically-controlled boundary layer cloud fraction is lowest during cold season over the eastern United States (Freedman et al., 2001). These results suggested that other physical processes, such as the snow albedo effect and snow/soil frozen/melting process may be more important to explain the surface temperature biases (Figure 6d).

Table 3. Relationships between solar radiation biases and air temperature biases during warm and cold season. The results are classified by clear sky index (CSI). The slope has been multiplied by scale factor of 1000. W indicates warm season, C indicates cold season.

CSI	[0, 0.2]	[0.2,0.3]	[0.3,0.4]	[0.4,0.5]	[0.5,0.6]	[0.6,0.7]	[0.7,0.8]	[0.8,0.9]	[0.9,1]
Slope(W)	4.77	4.26	3.96	3.73	3.53	3.45	2.97	2.61	2.25
r (W)	0.53	0.50	0.48	0.45	0.41	0.39	0.32	0.25	0.16
Slope (C)	1.74	1.53	0.45	-0.21	-0.77	-0.13	0.02	-0.22	-0.05
r (C)	0.09	0.09	0.03	-0.01	-0.04	-0.01	0.00	0.01	0.00

Figures 6e and 6f illustrates the interesting feature that extreme temperature biases larger than 5 K (assumed to be a temperature forecast error) is more frequent at 15:00 LT, typically considered to be the warmest time of day. However, another possible reason for the largest temperature biases may be associated with occasional afternoon thunderstorms, which occur around 15:00. The histogram of cold season extreme temperature biases are much flatter than during warm season, indicating that the frequency of extreme temperature bias does not correspond to the time of day as during the warm season.

4 Conclusions

One year of HRRR model and observation data were used in this study to investigate the biases from both diurnal and seasonal perspectives. The dense NYSM network (average distance between stations ~ 30 km) of 126 standard weather stations provides opportunities to investigate the impact of spatial heterogeneity on the land-atmosphere-cloud interaction as a coupled system.

First, an entire year of surface meterological fields was examined by separating the daily maximum and minimum temperature. Distinct physical processes governing diurnal and seasonal biases in the model were found. In the warm season, there are consistent warm and dry biases at 2 meter, with a relatively small standard deviation. At the diurnal scale, a negative correlation between biases in daily maximum and minimum temperature indicated that low-level clouds play an important role in the warm season surface warm and dry bias. Cold season biases show a much larger standard deviation but smaller mean biases. Furthermore, extreme cold biases exist in the nighttime in February, with large daytime wet biases in March. Understanding the role of snow is critical for the interpretation of cool season biases from both albedo and hydrological perspectives. The sensitivity of surface temperature to albedo during winter possibly creates the large variance in cold season biases. In the model, inaccurate partition between runoff and soil moisture from snowmelt may cause the wet bias from the late winter to early spring season.

Additionally, lacking a comprehensive representation of soil freezing-thawing processes, the model failed to predict a soil temperature barrier at the freezing point possibly a result of thermal inertia of freezing and thawing. These processes partly explain the extreme cold bias that occurred in February.

Taking advantage of the spatially densely distributed NYSM sites over heterogeneous land use types, statistical analysis is used to investigate further the land surface impact on the systematic warm and dry bias during the warm season, from temporal and spatial perspectives. Results suggest that the biases have two contributions. The first relates to the energy partition introduced by different land surface properties, and the second emerges from the model bias in cloud forcing. Statistics show that for the farmland sites, model overestimates the sensible heat flux and underestimates latent heat flux during the warm season, causing a 0.5 to 1 K warm bias and a 10% to 20% dry bias. On the contrary, the incorrect representation of energy budget over forest sites results in cold and wet biases under clear sky conditions.

Soil hydrological processes strongly control surface energy balance and fluxes, which are the most sensitive processes in the land surface model to the atmospheric model (Santanello et al., 2019). Through the whole year, soil moisture at all measured vertical levels (0.05, 0.25 and 0.5 m) are largely underestimated, contributing to the warm biases during the warm season. Also, this soil moisture underestimation reduces the soil heat capacity, causing the overestimation of soil temperature diurnal amplitude. We further analyzed the contribution of evapotranspiration and precipiatation to soil hydrological processes from seasonal perspective. Results show that during spring, the snow melting process controls the bias in soil moisture growth rate, leading to a $-0.004 m^3 m^{-3} h^{-1}$ interception in linear regression. During summer, the the soil moisture growth rate is underestimated due to the forecast shortfall in summer thunderstorm development. The soil moisture dry bias decreases from its maximum at the beginning of summer to much less in late summer (Figure 3c). The results indicate that evapotranspiration processes can be severely underestimated over the entire summer. The largest discrepancy is in the fall, when the model underpredicts the precipitation brought by tropical cyclones. In the meantime, the autumn evapotranspiration rate has been overestimated due to incorrect representation of seasonal transition when the leaves fall. The combined effect is a negative soil moisture of about 0.1 m^3/m^3 at the end of fall season. Winter biases mostly come from snow melting and soil freezing/thawing processes.

The dry bias in soil that appears during snow melt season is the main sources for the warm season soil moisture underestimation. The soil dries out in the model while the soil is moistened by melting snow in the observations. The water stress in the model soil hydrological processes plays an important role in the energy partition in the following summer season where the water stressed soil will inhibit the evapotranspiration and increase the Bowen ratio especially for shallow rooted vegetation, leading to the surface thermodynamic bias in the seasonal scales. These processes are amplified by the positive feedback loop between dry soil, reduced clouds, and warm temperatures. The positive feedback loop is most significant in warm season when the land surface atmosphere cloud coupling is strongest. This result presents a specific avenue for future model improvement: studying and improving the representation of snow melt and infiltration processes in the early spring.

Low-level clouds are recognized as one of the most important sources of the surface incident solar radiation and temperature biases. Complementing earlier analyses of the impact of sub-pixel cloud, we further explored the cloud effect by classifying cloud optical properties using

clear sky index directly calculated from NYSM measured incoming solar radiation. We found that the most optically thick clouds (generally associated with frontal system and thunderstorms) yielded the largest biases in solar radiation, the main contributor to the surface warm bias during the warm season. This finding emphasized the importance of further investigation of these clouds in the model.

The present work identifies HRRR model biases from the land-atmosphere coupling perspective. As an integrated system, biases of each feedback elements in land-atmosphere-cloud interactions can easily spread into the whole system and further increase the overall bias and reduce the forecast accuracy. For the future application of the HRRR model to forecast the alternate energy potential as well as for severe weather forecasting, our work identifies possible mechanisms responsible for the biases in the land surface processes, such as: soil hydrological, vegetation phenology, and thunderstorm development. However, the improvement of the land surface model is still challenging and requires better understanding of the physical processes as well as more complicated observation network and data assimilation techniques.

References

Benjamin, S. G., Weygandt, S. S., Brown, J. M., Hu, M., Alexander, C. R., Smirnova, T. G., et al. (2016), A North American hourly assimilation and model forecast cycle: The rapid refresh. *Monthly Weather Review*, *144*(4), 1669–1694. doi:10.1175/MWR-D-15-0242.1.

Betts, A. K., & Silva Dias, M. A. F. (2010), Progress in understanding land-surface-atmosphere coupling from LBA research. *Journal of Advances in Modeling Earth Systems*, *2*, 6, doi: 10.3894/JAMES.2010.2.6.

Betts, A. K., & Beljaars A. C. M. (2017), Analysis of near-surface biases in ERA-Interim over the Canadian Prairies. *Journal of Advances in Modeling Earth Systems*, *9*, 2158–2173. doi:10.1002/2017MS001025.

Brotzge, J. A., Wang, J., Thorncroft, C. D., Joseph, E., Bain, N., Bassill, N., et al. (2020), Technical overview of the New York State Mesonet Standard Network. *Journal of Atmospheric and Oceanic Technology*, 1–48, 1–48. doi:10.1175/JTECH-D-19-0220.1

Bytheway, J. L., Kummerrow, C. D., & Alexander, C. R. (2017), A Features-Based Assessment of the Evolution of Warm Season Precipitation Forecasts from the HRRR Model over Three Years of Development. *Weather and Forecasting*, *32*(5), 1841–1856. doi:10.1175/WAF-D-17-0050.1.

Covert, J. M. (2019), Design and Implementation of the New York State Mesonet Flux Tower Network. State University of New York at Albany, 99 pp. https://search.proquest.com/dissertations-theses/design-implementation-new-york-state-mesonet-flux/docview/2232975746/se-2?accountid=14166.

Ek, M. B., Mitchell, K. E., Lin, Y., Rogers, E., Grunmann, P., Koren, V., Gayno, G., & Tarpley, J. D. (2003), Implementation of Noah land surface model advances in the National Centers for Environmental Prediction operational mesoscale Eta model. *Journal of Geophysical Research*,

108(D22), 8851. doi:10.1029/2002JD003296.

Eltahir, E. A. B. (1998), A soil moisture–rainfall feedback mechanism 1. Theory and observations. *Water Resources Research*, *4*(34), 765–776.

Fitzjarrald, D. R., Acevedo, O. C., & Moore, K. E. (2001), Climatic consequences of leaf presence in the eastern United States. *Journal of Climate*, *14*, 598–614.

Freedman, J. M., Fitzjarrald, D. R., Moore, K. E., & Sakai, R. K. (2001), Boundary Layer Clouds and Vegetation-Atmosphere Feedbacks. *Journal of Climate*, *14*, 180–197.

Freedman, J. M., & Fitzjarrald, D. R. (2016), Mechanisms Responsible for the Observed Complex Structure in a Convective Boundary Layer Over the Hudson Valley. *Boundary-Layer Meteorology*, *164*, 89–106. doi: 10.1007/s10546-017-0241-6.

Garc´ıa-D´ıez, M., Fern´andez, J., Fita, L., & Yag¨ue, C. (2013), Seasonal dependence ofWRFmodel biases and sensitivity to PBL schemes over Europe. *Quarterly Journal of the Royal Meteorological Society*, *139*(671), 501–514. doi:10.1002/qj.1976.

Gascoin, S., Ducharne, A., Ribstein, P., Perroy, E., & Wagnon P. (2009), Sensitivity of bare soil albedo to surface soil moisture on the moraine of the Zongo glacier (Bolivia). *Geophysical Research Letters*, *36*, L02405. doi:10.1029/ 2008GL036377.

Griffin, S. M., Otkin, J. A., Rozoff, C. M., Sieglaff, J. M., Cronce, L. M., Alexander, C. R., Jensen, T. L., & Wolff, J. K. (2017), Seasonal analysis of cloud objects in the High-Resolution Rapid Refresh (HRRR) model using object-based verification. *Journal of Applied Meteorology and Climatolog*, *56*, 2317–2334. doi: 10.1175/JAMC-D-17-0004.1.

Iacono, M. J., Delamere, J. S., Mlawer, E. J., Shephard, M. W., Clough, S. A., & Collins, W. D. (2008), Radiative forcing by long–lived greenhouse gases: Calculations with the AER radiative transfer models. *Journal of Geophysical Research: Atmospheres*, *113*, D13103. doi:10.1029/2008JD009944 .

James, E. P., Benjamin, S. G., & Marquis, M. (2017), A unified high-resolution wind and solar dataset from a rapidly updating numerical weather prediction model. *Renewable Energy*, *102*(Part B), 390–405. doi:10.1016/j.renene.2016.10.059.

James, E., Ahmadov, R., & Grell, G. A. (2018), Realtime Wildfire Smoke Prediction in the United States: the HRRR-Smoke Model. *EGU General Assembly Conference Abstracts*, *20*, p. 19526.

Kala, J., De Kauwe, M. G., Pitman, A. J., Medlyn, B. E., Wang, Y.-P., Lorenz, R., & Perkins-Kirkpatrick, S. E. (2016), Impact of the representation of stomatal conductance on model projections of heatwave intensity. *Nature Science Report*, *6*, 23418. doi:10.1038/srep23418.

Katona, B., Markowski, P., Alexander, C., & Benjamin, S., (2016), The influence of topography on convective storm environments in the eastern United States as deduced from the HRRR.

Weather and Forecasting, *31*(5), 1481–1490. http://dx.doi.org/10.1175/WAF-D-16- 0038.1.

Koster, R. D., et al. (2004), Regions of strong coupling between soil moisture and precipitation. *Science*, *305*, 1138–1140. doi:10.1126/ science.1100217.

Koster, R. D., et al. (2006), GLACE: The global land-atmosphere coupling experiment. Part I: Overview. *Journal of Hydrometeorology*, *7*(4), 590–610.

Lee, T. R., Buban, M., Turner, D. D., Meyers, T. P., & Baker, B. (2019), Evaluation of the High-Resolution Rapid Refresh (HRRR) Model Using Near-Surface Meteorological and Flux Observations from Northern Alabama. *Weather and Forecasting*, *34*, 635–663. doi: 10.1175/WAF-D-18-0184.1.

Min, Q. L., & Harrison, L. C. (1996), Cloud properties derived from surface MFRSR measurements and comparison with GOES results at the ARM SGP site, *Geophysical Research Letters*, *23*, 1641.

Mueller, B., & Seneviratne, S. I. (2014), Systematic land climate and evapotranspiration biases in CMIP5 simulations. *Geophysical Research Letters*, *41*, 128–134. doi:10.1002/2013GL058055.

Olson, J. B., Kenyon, J. S., Angevine, W. M., Brown, J. M., Pagowski, M., & Sušelj, K. (2019), A Description of the MYNN-EDMF Scheme and the Coupling to Other Components in WRF–ARW. *NOAA Technical Memorandum OAR GSD*, *61*, pp. 37. doi:10.25923/n9wm-be49.

Peters, J. M., Nielsen, E. R., Parker, M. D., Hitchcock, S. M., & Schumacher, R. S. (2017), The Impact of Low-Level Moisture Errors on Model Forecasts of an MCS Observed during PECAN. *Monthly Weather Review*, *145*(9), 3599–3624. doi: 10.1175/MWR-D-16-0296.1.

Pichugina, Y. L., et al., (2017), Assessment of NWP forecast models in simulating offshore winds through the lower boundary layer by measurements from a ship-based scanning Doppler lidar. *Monthly Weather Review*, *145*(10), 4277–4301. doi: 10.1175/MWR-D-16-0442.1.

Pleim, J., & Ran, L. (2011), Surface flux modeling for air quality applications. *Atmosphere*, *2*(3), 271–302. doi:10.3390/atmos2030271.

Robledo, L. & Soler, A. (2000), Luminous efficacy of global solar radiation for clear skies. *Energy Conversion and Management*, *41*(2000), 1769–1779.

Schar, C., Luthi, D., Beyerle, U., & Heise, E. (1999), The soil-precipitation feedback: A process study with a regional climate model. *Journal of Climate*, *12*(3), 722–741.

Seneviratne, S. I., Corti, T., Davin, E. L., Hirschi, M., Jaeger, E. B., Lehner, I. et al . (2010), Inverstigating soil moisture−climate interactions in a changing climate: a review. *Earth-Science Reviews*, *99*(3-4), 125–161. doi:10.1016/j.earscirev.2010.02.004.

Seneviratne, S. I., et al. (2013), Impact of soil moisture–climate feedbacks on CMIP5 projections: First results from the GLACE-CMIP5 experiment. *Geophysical Research Letters*,

40, 5212–5217. doi: 10.1002/grl.50956.

Smirnova, T. G., Brown, J. M., & Benjamin, S. G. (1997), Performance of Different Soil Model Configurations in Simulating Ground Surface Temperature and Surface Fluxes. *Monthly Weather Review*, *125*(8), 1870–1884. doi: 10.1175/1520-0493(1997)125<1870:PODSMC>2.0.CO;2.

Smirnova, T. G., Brown, J. M., Benjamin, S. G., & Kenyon, J. S. (2016), Modifications to the Rapid Update Cycle Land Surface Model (RUC LSM) Available in the Weather Research and Forecasting (WRF) Model. *Monthly Weather Review*, *144*(5), 1851–1865. doi: 10.1175/MWR-D-15-0198.1

Steeneveld, G. J., Tolk, L. F., Moene, A. F., Hartogensis, O. K., Peters, W.,& Holtslag, A. A. M. (2011), Confronting the WRF and RAMS mesoscale models with innovative observations in the Netherlands: Evaluating the boundary layer heat budget. *Journal of Geophysical Research: Atmospheres*, *116*, D23114. doi:10.1029/2011JD016303.

Stull, R. B., (1988), An Introduction to Boundary Layer Meteorology. Netherlands: Springer.doi: 10.1007/978−94−009−3027−8_7.

Sun, X., Holmes, H. A., Osibanjo, O. O., Sun, Y., Cesunica E., & Ivey, C. E. (2017), Evaluation of Surface Fluxes in the WRF Model: Case Study for Farmland in Rolling Terrain. *Atmosphere*, *8*(10), 197. doi:10.3390/atmos8100197.

Taylor, C. M., Richard, D. A. M., Guichard, F., Harris, P. P. & Dorigo, W. A. (2012), Afternoon rain more likely over drier soils. *Nature*, *489*, 423–426. doi:10.1038/nature11377

Thompson, G., & Eidhammer, T. (2014), A study of aerosol impacts on clouds and precipitation development in a large winter cyclone. *Journal of the Atmospheric Sciences*, *71*(10), 3636–3658. doi:10.1175/ JAS-D-13-0305.1.

Wagner, T., P. Klein, & Turner, D. (2019), A new generation of ground-based mobile platforms for active and passive profiling of the boundary layer. *Bulletin of the American Meteorological Society*, *100*(1), 137–153. doi: 10.1175/BAMS-D-17-0165.1.

Williams, I. N., Lu, Y., Kueppers, L. M., Riley, W. J., Biraud, S. C., Bagley, J. E. & Torn, M. S. (2016), Land-atmosphere coupling and climate prediction over the U.S. Southern Great Plains. *Journal of Geophysical Research: Atmospheres*, *121*, 12125–12144. doi:10.1002/2016JD025223.

Yang, J., & Min, Q. (2018), Retrieval of atmospheric profiles in the New York State Mesonet using one-dimensional variational algorithm. *Journal of Geophysical Research: Atmospheres*, *123*, 7563–7575. doi: 10.1029/ 2018JD028272.

Min, Q. L., and L. C. Harrison (1996), Cloud properties derived from surface MFRSR measurements and comparison with GOES results at the ARM SGP site, *Geophys. Res. Lett.*, *23*, 1641.

Viterbo, P., Beljaars, A., Mahfouf, J. F., & Teixeira, J. (1999), The representation of soil moisture

freezing and its impact on the stable boundary layer. *Quarterly Journal of the Royal Meteorological Society*, *125*(559), 2401–2426. doi: 10.1002/qj.49712555904.